EUROPEAN JOURNAL OF MATERIALS SCIENCE AND ENGINEERING
Volume 4, Issue 3, 2019: 103-113 | www.ejmse.tuiasi.ro | ISSN: 2537-4338

EJMSE

DOI: 10.36868/ejmse.2019.04.03.103

EFFECT OF ENERGY DENSITY AND BUILD ORIENTATION ON MICROSTRUCTURE OF ADDITIVE MANUFACTURED STAINLESS STEEL

Penn RAWN, Vadiraja SUDHAKAR*

[1]Montana Technological University, Butte, MT 59701, USA

Abstract

The objective of the present investigation was to evaluate microstructures of 316L stainless steel produced by laser powder bed fusion (LPBF) processing, as a function of processing parameters (specifically, build angle orientations and global energy density). Microstructures were characterized using an optical microscope attached with a software for a detailed analysis. Microstructure studies revealed that the grain size was only marginally affected by the build angle orientation. Micro-voids were minimal and almost no unmelted particles were noticed at relatively higher GED values, due to more complete melting conditions.

Keywords*: Microstructure, 316L stainless steel, laser powder bed fusion processing (LPBF), global energy density.*

Introduction

Laser powder bed fusion processing (LPBF) is one of the types of Laser additive manufacturing (LAM) processing that involves the production of 3D components by heating the powder bed, layer by layer using laser energy. The loss of minimal material and the production of complex shapes with desired mechanical properties are some of the highlights of this process [1]. It is well known that austenitic stainless steels are difficult and expensive to machine because of their higher hardenability characteristics. So, additive manufacturing is a better option for producing engineering components made of austenitic stainless steels. Austenitic stainless steels are also known to undergo sensitization when are fabricated by welding process. Also welding may produce corrosion sensitive grain boundaries [2]. Austenitic stainless steel grade 316L, offers excellent corrosion resistance, especially in marine environments [3]. Low carbon grade of austenitic stainless steel (316L SS) is free from weld decay or sensitization issues [4]. LAM process is typically used to produce a high density product with reduced porosity. However, the high laser energy input could lead to many solidification defects including distortion and subsequent cracking [5].

Solidification defects are common in LAM processing due to high laser power used. High laser energy input also leads to defects like faceted voids, porosity, inclusions, micro-cracks, balling, and denudation zones [6-9]. Distortion of the LAM processed component could also result in micro-cracking and bending stress in them [10]. Gas porosity that are spherical in shape occurs due to entrapped air in the powder bed [11-14]. On the other hand, non-spherical pores or the faceted voids usually occur due to lack of fusion leading to the formation of unmelted particles [15-16]. The objective of the present study is to characterize the microstructural details of 316L stainless steel [17] as a function of build angle orientations and global energy density.

Corresponding author: kvsudhakar@mtech.edu

Materials and Methods

Material and LPBF processing parameters

The chemical composition of the 316L stainless steel used in the present investigation is shown in Table 1.

Table 1. Chemical composition of Stainless Steel (AISI 316L grade) [17]

Element	C	Cr	Ni	Mo	Co	Si
Wt.%	0.02	16.9	12.1	2.4	0.06	0.5

Energy density, a key processing variable, was calculated using the following equation (1);

$$E = \frac{P}{vh} \tag{1}$$

Where, P is the laser power in watt, v is the travel speed in mm/s, h is the hatch spacing in mm. Layer thickness in mm, was kept constant in the present study.

Microstructure characterization

Microstructures of stainless steel were examined after etching with Kalling's reagent (5 g $CuCl_2$, 100 ml HCl, and 100 ml Ethanol) and Villella's reagent (1 g Picric acid, 5 ml HCl, 100 ml Ethanol), separately.

Results and Discussion

Effect of microstructure on energy density

Table 2 shows the details regarding the build parameters (process variables) in terms of the energy density. It may be noted that while energy density is varied, the specimen build angle orientation was kept constant, at 90°. In these experiments, factorial design matrix was used that had a two-level, three sets of parameters.

Table 2. Build parameters used including global energy density [17]

Sample Label	Laser Power (P), W	Scan Speed (v), mm/s	Hatch Spacing (h), mm	Energy Density, ED (P/vh, J/mm^2)
S-1	156	866.4	0.072	2.50
S-2	234	866.4	0.072	3.75
S-3	156	1299.6	0.072	1.67
S-4	234	1299.6	0.072	2.50
S-5	156	866.4	0.108	1.67
S-6	234	866.4	0.108	2.50
S-7	156	1299.6	0.108	1.11
S-8	234	1299.6	0.108	1.67

Table 3 summarizes the details for specimens having relatively higher and lower values of processing variables used in the present investigation.

A typical LPBF processed austenitic stainless steel's microstructure is demonstrated in Fig. 1a. The microstructure reveals the presence of melt pool boundaries and columnar/cellular structures including porosity. Higher resolution image of the cellular structures with porosity/inclusions, shown in Fig. 1.b).

Table 3. Build parameters selected for comparison

Parameter	Lower range of Energy Density	Higher range of Energy Density
Power	S-1	S-2
	S-3	S-4
	S-5	S-6
Travel Speed	S-1	S-3
	S-6	S-8
	S-2	S-4
Hatch Spacing	S-1	S-5
	S-2	S-6
	S-4	S-8

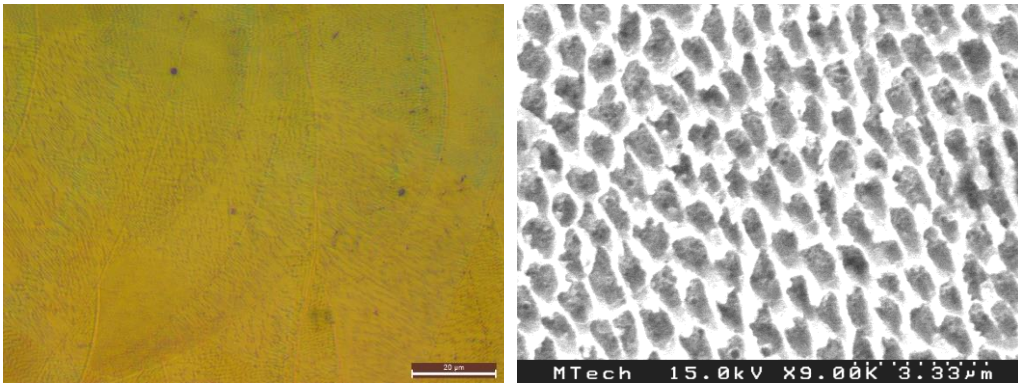

a) b)

Fig. 1. Optical microstructure of sample S-1: a) showing melt pool boundaries with dendrites/cellular structure; b) SEM micrograph image showing cellular structure with porosity

Fig. 2 shows relatively a more stretched grains/cells.

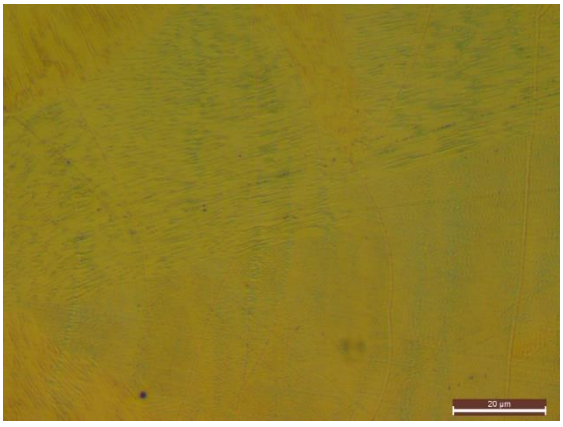

Fig. 2. Optical microstructure showing elongated cells/grains for sample S-1

Microstructure of the sample S-2 that was produced using the highest energy density is shown in Fig. 3.a) with relatively coarser columnar dendritic/cellular microstructure. Columnar morphology appears anisotropic. Fig. 3.b) depicts the presence of porosity.

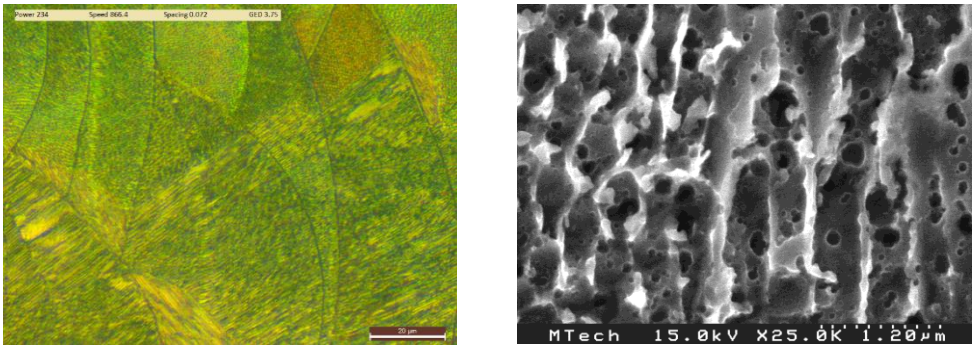

a) b)

Fig. 3. Optical micrograph of sample S-2: a) showing coarser columnar structure; b) SEM micrograph revealing porosity

The columnar structure of the sample S-3 shown in Fig. 4.a), is relatively shorter and wider, and finer cellular structure, in comparison to that for sample S-1. Fig. 4.b) illustrates the presence of denudation zones in isolation.

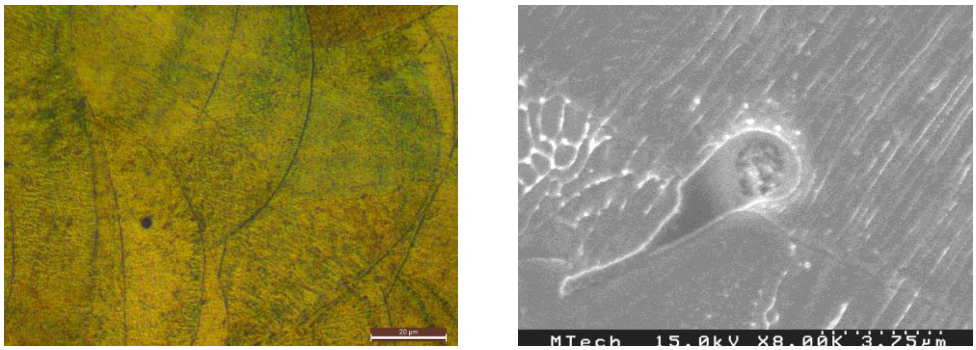

a) b)

Fig. 4. Optical micrograph of sample S-3: a) showing shorter columnar and finer cellular structure; b) SEM micrograph revealing denudation zone

Relatively coarser microstructure for the sample S-4 is revealed in Fig. 5. A highly directional dendritic structure can be seen along with discontinuities such as pores and inclusions.

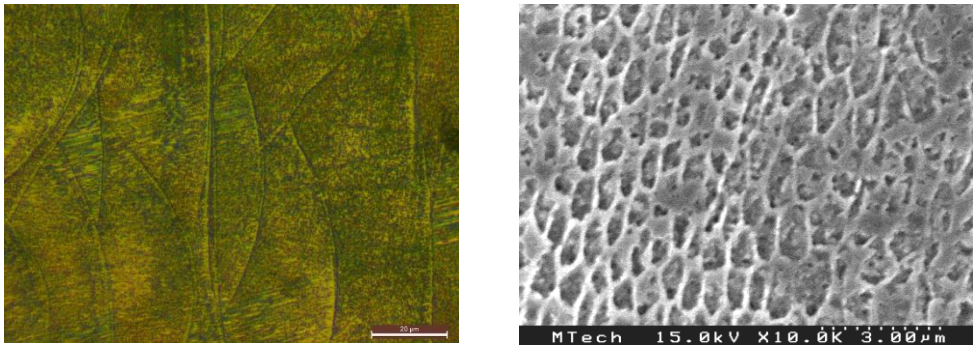

a) b)

Fig. 5. Optical micrograph of sample S-4: a) showing coarser columnar structure; b) SEM micrograph revealing porosity and inclusions

The coarse microstructure of sample S-5 is presented in Fig. 6.a) with dendrites relatively shorter than for sample S-4, but with no voids. Multiple-oriented dendritic structures are demonstrated using an SEM micrograph, as shown in Fig. 6.b).

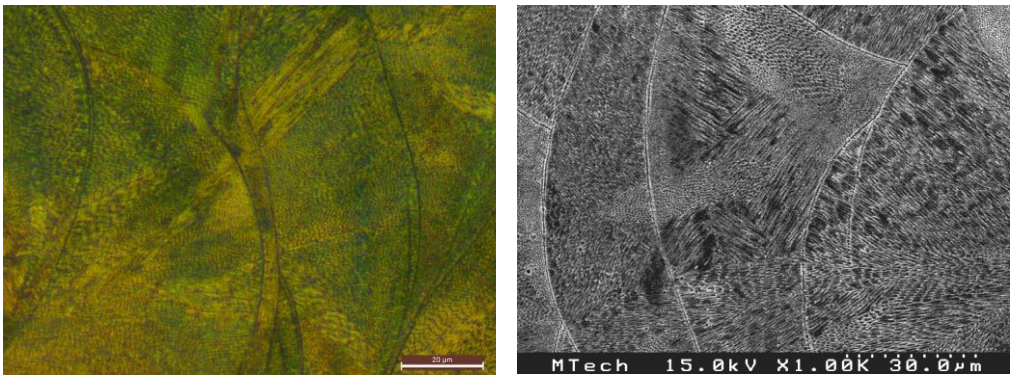

a) b)

Fig. 6. Optical micrograph of sample S-5: a) showing coarser, but shorter columnar structure; b) SEM micrograph showing multiple-growth directions of dendrites

Fig. 7.a), corresponding to sample S-6, shows relatively a fewer dendritic/cellular structure as compared to the previously described samples. SEM micrograph (as shown in Fig. 7.b) reveals a denudation zone [18].

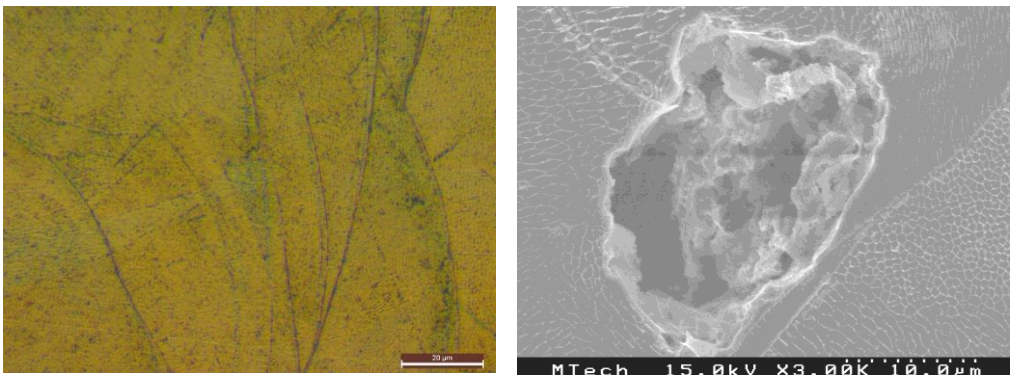

a) b)

Fig. 7. Optical micrograph of sample S-6: a) showing a few dendritic structures; b) SEM micrograph showing a denudation zone

Many faceted voids are demonstrated in Fig. 8.a), corresponding to sample S-7, that was produced with the lowest energy density. Fig. 8.b) shows a few unfused powder particle inside those faceted voids.

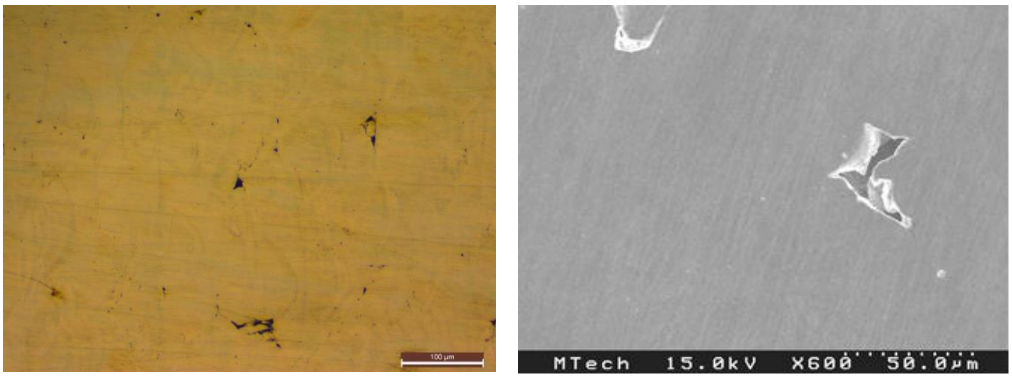

a) b)

Fig. 8. a) Optical micrograph of sample S-7, showing many faceted voids;
b) SEM micrograph revealing unfused powder particles during laser melting

Fig. 9.a) (for sample S-8) shows relatively the finest microstructure of all the samples, with an isolated void. SEM micrograph (Fig. 9.b) shows a solidification cracking surrounded by a columnar/cellular structure.

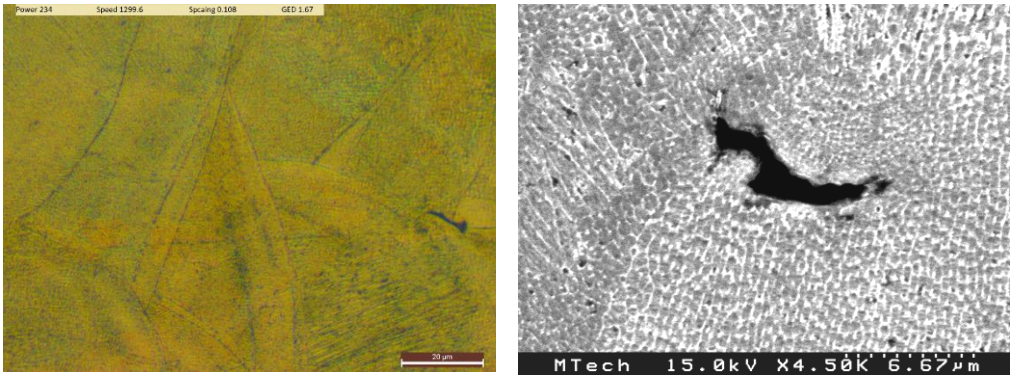

a) b)

Fig. 9. Optical micrograph of sample S-8: a) showing the finest microstructure;
b) SEM micrograph revealing solidification cracking

Microstructure as a function of build angle orientation

Finer columnar/cellular microstructures are shown Fig. 10a, for the sample with 0° build angle orientation. Fig. 10.b) an SEM micrograph, shows denudation zones. Denudation zone refers to the depletion of metal powder particles in the zone immediately surrounding the solidified track, and is due to a competition between outward metal vapor flux directed away from the laser spot and entrainment of powder particles in a shear flow of gas driven by a metal vapor jet at the melt track [19-21].

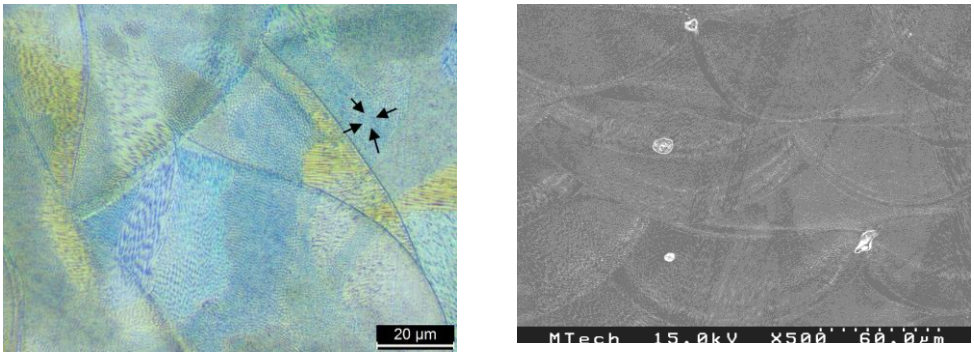

a) b)

Fig. 10. a) Optical micrograph of a 0° build angle orientation sample revealing a finer microstructure; b) SEM micrograph revealing denudation zones

Denudation zone in another location for the metal is seen for the 0° orientation sample is revealed in Fig. 11.

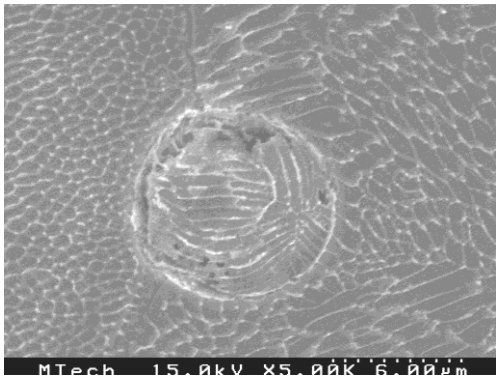

Fig. 11. SEM micrograph of 0° orientation sample showing a denudation zone in another location

Finer and coarser cellular structures for the 30° build angle orientation sample is shown in Fig. 12.a) and Fig. 12.b) reveals balling, a defect due to the liquid-gas interfacial tension.

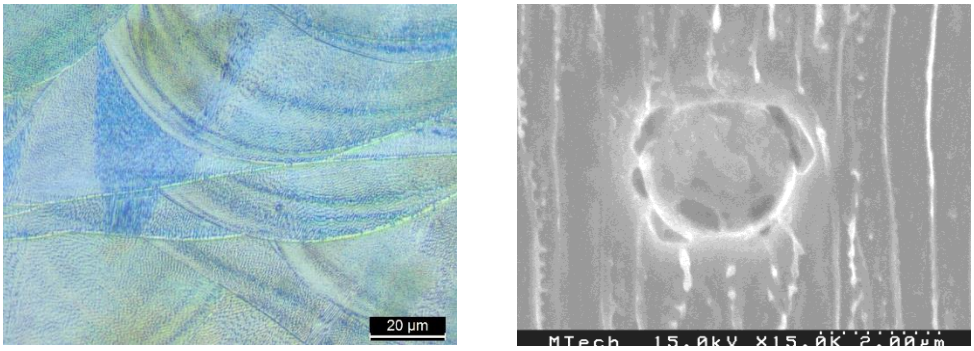

a) b)

Fig. 12. a) Optical micrograph of a 30° build angle orientation sample showing both finer and coarser microstructure; b) SEM micrograph showing a balling discontinuity

Fig. 13 shows a denudation zone for the sample described in Fig. 12.

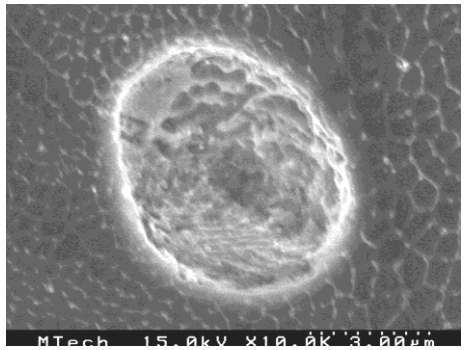

Fig. 13. SEM micrograph showing a denudation zone

The microstructure of the sample with 60° orientation is shown in Fig. 14.a) which is almost similar to 30° orientation sample. Fig. 14.b) shows micro-cracking, and the microstructure features are similar to the one that was shown in Fig. 12.

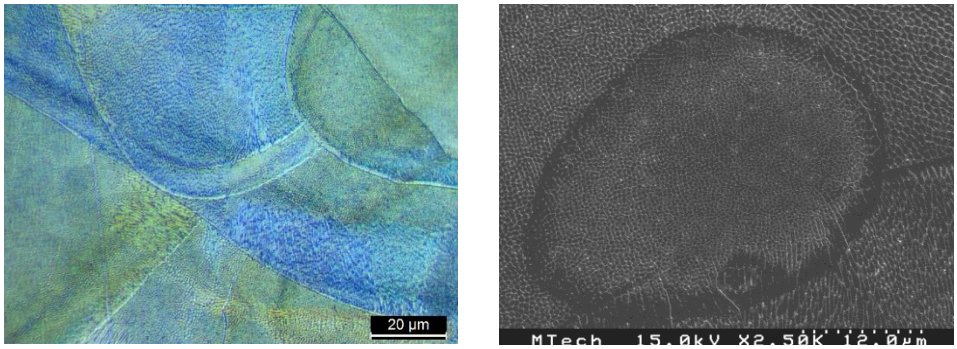

a) b)

Fig. 14. a) Optical micrograph of a 60° build angle orientation sample showing both finer and coarser microstructure; b) SEM micrograph showing a balling discontinuity

Fig. 15 shows a large faceted void that coincides with the melt pool boundaries, for the 60° build orientation sample.

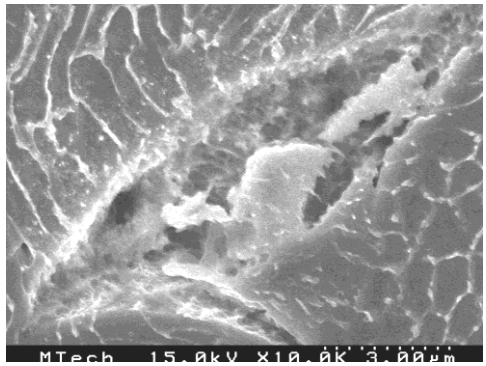

Fig. 15. SEM micrograph revealing a large faceted void for the 60° oriented sample

Fig. 16.a) shows a combination of finer dendrites and cellular structures for the 90^0 oriented sample. Faceted voids are shown in an SEM image of Fig. 16.b).

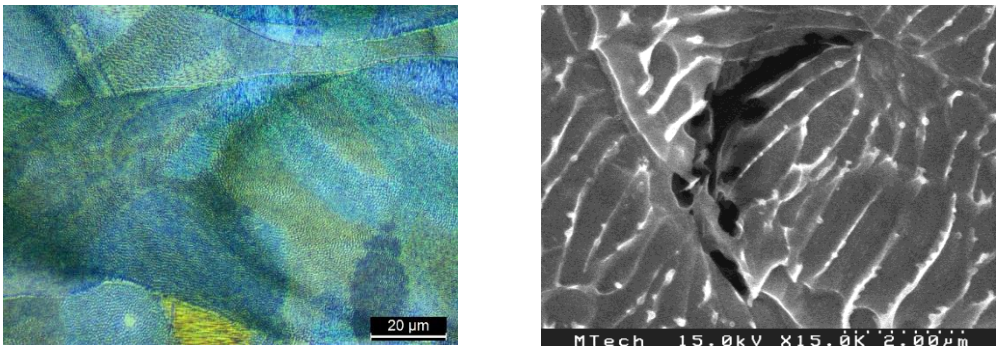

a) b)

Fig. 16. a) Optical micrograph of a 90° build angle orientation sample showing very fine cellular microstructure; b) SEM micrograph showing faceted voids

Fig. 17. SEM micrograph revealing balling defect for the 90° orientation sample

Similar to the defects shown in Fig. 12 and Fig. 14, 90° orientation sample also revealed a balling defect, as shown in Fig. 17.

Conclusions

Overall grain size of the samples was affected by the specimen angle orientations, but the orientations had only a marginal effect on the mean grain size

Higher energy density samples showed relatively coarser cellular structure with highly aligned dendritic morphology

At relatively lower energy densities, several large faceted voids were observed with unfused powder particles within the voids

The voids were minimal and almost no unfused/unmelted particles were noticed at relatively higher energy densities

A combination of fine and coarse cellular structures were observed for 30° build angle orientation samples as opposed to only very fine cellular or dendritic structures for the 0° orientation samples

Microscopic studies revealed the presence of discontinuities like denudation zones, balling, faceted voids, and spherical pores in LPBF processed 316L stainless steel

Acknowledgement

Research was sponsored by the Army Research Laboratory and was accomplished under Cooperative Agreement Number W911NF-15-2-0020. The views and conclusions contained in this document are those of the authors and should not be interpreted as representing the official policies, either expressed or implied, of the Army Research Laboratory or the U.S. Government. The U.S. Government is authorized to reproduce and distribute reprints for Government purposes notwithstanding any copyright notation herein.

The authors are grateful to Mr. Gary Wyss, Senior Scientist, CAMP, for SEM analysis, Ronda Coguill for the support on tensile test specimens, and Dr. Bruce Madigan, Professor.

References

[1] K. Shahzad, J. Deckers, J.P. Kruth, J. Vleugels, *Additive manufacturing of alumina parts by indirect selective laser sintering and post processing*, **Journal of Materials Processing and Technology**, **213**, 2013, pp. 1484–1494.

[2] R.W.K. Honeycombe, H.K.D.H. Bhadeshia, *Steels – microstructure and properties*. 2nd ed. London: Edward Arnold,1995.

[3] A.J. Sedriks, *Corrosion resistance of austenitic Fe–Cr–Ni–Mo alloys in marine environments*, **International Material Reviews**, **27**, 1982, pp. 321–353.

[4] T.M. Devine, C.L. Briant, B.J. Drummond, *Mechanism of intergranular corrosion of 316l stainless steel in oxidizing acids*, **Scripta Metallurgica**, **14**, 1980, pp. 1175–1179.

[5] V. Manvatkar, A. De, T. DebRoy, Heat transfer and material flow during laser assisted multi-layer additive manufacturing, **Journal of Applied Physics**, 2014, 116 (12), doi:10.1063/1.4896751.

[6] D.C. Holly, Abdel Haboub, G.F. Gallegos, D.Y. Parkinson, A.A. MacDowell, *Damage evolution and failure mechanisms in additively manufactured stainless steel*, **Materials Science and Engineering: A**, **651**, 2016, pp. 406–414.

[7] S. A. Khairallah, A.T. Anderson, A. Rubenchik, W.E. King, *Laser powder-bed fusion additive manufacturing: Physics of complex melt flow and formation mechanisms of pores, spatter, and denudation zones*, **Acta Materialia**, **108**, 2016, pp. 36–45.

[8] Z. Sun, X. Tan, S.B. Tor, W.Y. Yeong, *Selective laser melting of stainless steel 316L with low porosity and high build rates*, **Materials & Design**, **104**, 2016, pp. 197–204.

[9] Z. Wang, T.A. Palmer, A.M. Beese, *Effect of processing parameters on microstructure and tensile properties of austenitic stainless steel 304L made by directed energy deposition additive manufacturing*, **Acta Materialia**, **110**, 2016, pp. 226–235,

[10] B. Song, X. Zhao, S. Li, C. Han, Q. Wei, *Differences in microstructure and properties between selective laser melting and traditional manufacturing for fabrication of metal parts: A review*, **Frontiers of Mechanical Engineering**, **10(2)**, 2015, pp. 111–125.

[11] Y.F. Shen, D.D. Gu, P. Wu, *Development of porous 316L stainless steel with controllable microcellular features using selective laser melting*, **Materials Science and Technology**, **24(12)**, 2008, pp. 1501–1505.

[12] T.M. Mower, M.J. Long, *Mechanical behavior of additive manufactured, powder-bed laser-fused materials*, **Materials Science and Engineering: A**, 2016, **651**, pp. 198–213.

[13] M. Ma, Z. Wang, M. Gao, X. Zeng, *Layer thickness dependence of performance in high-power selective laser melting of 1Cr18Ni9Ti stainless steel*, **Journal of Materials Processing Technology**, **215**, 2015, pp. 142–150.

[14] R. Boom, A.A. Kamperman, O. Dankert, *Argon solubility in liquid steel*, **Metallurgical and Materials Transactions B**, **31**, 2000, pp. 913-919.

[15] J. P. Kruth, J. Deckers, E. Yasa, *Assessing and comparing influencing factors of residual stresses in selective laser melting using a novel analysis method*, **Proceedings of the Institution of Mechanical Engineers, Part B: Journal of Engineering Manufacture**, **226(6)**, 2012, pp. 980–991.

[16] J.A. Cherry, H.M. Davies, S. Mehmood, N.P. Lavery, S.G.R. Brown, J. Sienz, *Investigation into the effect of process parameters on microstructural and physical properties of 316L stainless steel parts by selective laser melting*, **Springer Link**, Springer London, 2014, link.springer.com/article/10.1007/s00170-014-6297-2.

[17] P. Rawn, *3D Printing of 316L Stainless Steel and its Effect on Microstructure and Mechanical Properties*, https://digitalcommons.mtech.edu/grad_rsch/140, 2017, pp. 1-88.

[18] Y. Zhong, L. Liu, S. Wikman, D. Cui, *Intragranular cellular segregation network structure strengthening 316L stainless steel prepared by selective laser melting*, **Journal of Nuclear Materials**, **470**, 2016, pp. 170–178.

[19] M. J. Matthews, G. Guss, S. A. Khairallah, A. M. Rubenchik, P. J. Depond, W. E. King, *Denudation of metal powder layers in laser powder bed fusion processes*, **Acta Materialia**, **114**, 2016, pp. 33-42.

[20] Y. Adroitsev, P. Bertrand, G. Antonenkova, I. Smurov, *Use of track/layer morphology to develop functional parts by selective laser melting*, **Journal of Laser Applications**, **25(5)**, 2013, doi: 10.2351/1.4811838.

[21] R. Gusarov, I. Yadroitsava, I. Smurov, I. Yadroitsev, *Single track formation in selective laser melting of metal powders*, **Journal of Materials Processing and Technology**, **210(12)**, 2010, pp. 1624-1631.

Received: December 13, 2019
Accepted: January 21, 2019